Author/s:
Patterson, JW;Driesner, T;Matthai, S;Tomlinson, R

Title:
Heat and Fluid Transport Induced by Convective Fluid Circulation Within a Fracture or Fault

Date:
2018-04-01

Citation:
Patterson, J. W., Driesner, T., Matthai, S. & Tomlinson, R. (2018). Heat and Fluid Transport Induced by Convective Fluid Circulation Within a Fracture or Fault. Journal of Geophysical Research Solid Earth, 123 (4), pp.2658-2673. https://doi.org/10.1002/2017JB015363.

Persistent Link:
https://hdl.handle.net/11343/283859

Patterson James, W. (Orcid ID: 0000-0003-2950-2867)
Driesner Thomas (Orcid ID: 0000-0002-9413-4389)

Heat and fluid transport induced by convective fluid circulation within a fracture or fault

J.W. Patterson[1], T. Driesner[1], S. Matthai[2], R. Tomlinson

[1]Department of Earth Sciences, Swiss Federal Institute of Technology Zurich, Zurich, Switzerland

[2]Department of Infrastructure Engineering, University of Melbourne, Melbourne, Australia

Corresponding author: James Patterson (james.patterson@erdw.ethz.ch)

Key points:

- Fluid convection in buried fracture zones can lead to significant heat flow focusing
- Transmissivity, rather than thickness or permeability alone, controls convective patterns in the fracture and related thermal anomalies
- Interaction between convection in fracture and permeable hosts is a function of host rock permeability

This is the author manuscript accepted for publication and has undergone full peer review but has not been through the copyediting, typesetting, pagination and proofreading process, which may lead to differences between this version and the Version of Record. Please cite this article as doi: 10.1002/2017JB015363

Abstract:

Natural water convection in subvertical fractures, fracture zones, or faults can perturb the temperature field around the fracture and enhance and focus vertical heat flow within. We investigate, by means of numerical simulation, the effects of convection in a deeply buried vertical fracture zone. Fracture zone transmissivity, defined as permeability times thickness of the permeable region, is found to be the primary control on convection style rather than fracture zone thickness or permeability alone. In an impermeable host rock, the convection-induced thermal anomaly propagates solely via conduction, diminishing away from the fracture. Convective heat flow increases with fracture transmissivity up to ca. 10^{-8} m^3, when a plateau in convective heat flow is reached, constrained by fracture size and the host rock's thermal conductivity. Permeable host rocks modify these results significantly. In a moderately permeable host rock (10^{-14} m^2), convection in the fracture induces non-Rayleigh fluid convection, while thermal effects and fluid exchange between host rock and fracture remain moderate. If the host rock is sufficiently permeable to allow porous medium Rayleigh convection to occur (10^{-13} m^2), the convection patterns within the fracture are overprinted by the host's convective patterns. Fluid exchange between the fracture and the rock will be significant. Our findings provide insight into how thermal anomalies in the uppermost crust may relate to locally enhanced heat flow from convection in non-outcropping fractures below. Furthermore, the results for permeable host rocks provide evidence for previously inferred hydrologic scenarios for the formation of certain hydrothermal, vein-type mineral deposits.

1 Introduction:

Fractures and faults are common features of the shallow crust and often serve as high-permeability conduits for fluid, heat, and solute transport [Lowell 1975; Berkowitz 2002; Simms and Garven 2004]. Fluid is focused into these features, impacting subsurface heat distribution [Waring 1983] and promoting fluid mixing, which may result in localized ore deposition [Koide and Bhattacharji 1975; Haynes et al. 1995; Matthäi, Heinrich, and Driesner 2004; Ingebritsen and Appold 2012] or diagenesis [Chan, Parry, and Bowman 2000; Eichhubl, Davatzes, and Becker 2009]. It is well known that convective flow of fluid may occur in fractures and faults, significantly increasing heat transport through the system [Lowell 1975; Murphy 1979; Rabinowicz 1999; Faulds et al. 2010].

A prominent example for the importance of natural fracture-bound fluid convection (hereby referred to as "fracture convection") is the Soultz-sous-Fore□ts Enhanced Geothermal System test site in France [Clauser, Griesshaber, and Neugebauer 2002; Bächler, Kohl, and Rybach 2003; Genter et al. 2010]. There, a significant thermal anomaly and large geothermal gradients in the sedimentary cover give way to gradients as low as 10°C/km in the granitic basement at 1.4 to 3.7 km depth [Pribnow and Schellschmidt 2000]. Such low gradients cannot be explained solely by conductive heat transfer as this would require thermal conductivities much higher than those of the basement; rather they are interpreted as the consequence of fluid convection in fractures in otherwise essentially impermeable granitic rocks [Genter et al. 2010; Siffert et al. 2013]. Equivalent porous medium permeability of the unstimulated fractured granite has been estimated to be on the order of 10^{-17} m^2 [Rummel 1991; Evans, Genter, and Sausse 2005], too low for natural convection in a purely porous medium [Ingebritsen et al. 2010]. This discrepancy calls for a more quantitative assessment of the role of fracture convection in crustal heat transport.

Previous studies have taken into account heat exchange between convection within a single planar fracture or fault and host rock walls, both in 2D [Sorey 1978; Murphy

1979] and 3D [López and Smith 1995]. These earlier works focused on stability analysis and convective regimes, while López [2002] investigated the resultant thermal perturbation in the host rock. More recent studies focused on this thermal effect, but consider only a 2D domain [Guillou-Frottier et al. 2013], which does not account for convection cells within the fracture plane.

Fracture convection can induce fluid movement in the host rock, via fluid exchange between fracture and host [Magri et al. 2016] or by inducing convection due to lateral thermal gradients [Wangen 1997]. This fracture-matrix exchange is often accounted for in 2D convection models [Jianwen Yang, Latychev, and Edwards 1998; Simms and Garven 2004], but sparingly in 3D models [López and Smith 1995; Bächler, Kohl, and Rybach 2003]. All of these studies have focused on surface-connected features. Localized hot and cold regions are created by Rayleigh convection within a fracture, resulting in lateral temperature gradients within and laterally away from the fracture [Bächler, Kohl, and Rybach 2003; Guillou-Frottier et al. 2013]. These lateral thermal gradients can induce convection in the host rock, causing fluid to buoyantly rise or sink. Rayleigh-Bérnard convection is the result of vertical temperature gradients; therefore, this lateral gradient-driven convection is referred to as "non-Rayleigh" convection [Wangen 1997; Simms and Garven 2004].

The role of fractures in uniform, permeable rock units undergoing Rayleigh convection has been studied in 2D [Pedersen and Bjørlykke 2007; J. Yang, Large, and Bull 2004; Guillou-Frottier et al. 2013], while convection patterns within a fault have been studied in 3D [Bächler, Kohl, and Rybach 2003]. However, to the best of our knowledge, the simultaneous natural convection in fractures/faults and host rock has not been investigated systematically, except by Tomlinson who, in contrast to this study, only considered the temperature dependence of fluid density using the Boussinesq approximation [Tomlinson 2006]. Natural convection within a permeable host rock (hereby referred to as "host rock convection") has been thoroughly studied [e.g., Holst and Aziz 1972; Nield and Bejan 2006], but little is understood of how fracture convection may affect it.

This study attempts to begin filling these knowledge gaps about natural convection in and around fractures. By means of numerical simulation, the thermal effects of fracture convection in a single fracture, entirely embedded in impermeable host rock and without connection to the surface, are investigated. In particular we look at the additional heat transported through the fracture to overlying rock units. Next, the host rock permeability is increased and non-Rayleigh convection is investigated, focusing on flow patterns into, out of, and around the convecting fracture. Lastly, host rock permeability is increased such that natural convection is initiated in both fracture and the permeable rock layer.

2 Methodology

Single-phase fluid flow in a porous medium is commonly described by Darcy's law:

$$\boldsymbol{v} = -\frac{k}{\mu_f}\left(\nabla p - \rho_f \boldsymbol{g}\right), \quad (1)$$

where $\boldsymbol{v}$ is the fluid velocity vector, k is rock permeability, μ_f is dynamic fluid viscosity, p is fluid pressure, ρ_f is fluid density, and $\boldsymbol{g}$ is the gravitational acceleration vector. The permeability of an open slot fracture is often approximated by the parallel plate assumption, calculated [Bear 1972; Witherspoon et al. 1980] as:

$$k = \frac{a^2}{12}, \quad (2)$$

where a is parallel plate fracture aperture. Combining Darcy's law with a mass-based continuity equation leads to the transient fluid pressure equation (e.g., Yapparova et al. 2014)

$$\left((1-\phi)\rho_f\beta_f + \phi\rho_r\beta_r\right)\frac{\partial p}{\partial t} = \nabla\cdot\left(\rho_f\frac{k}{\mu_f}\left(\nabla p - \rho_f\boldsymbol{g}\right)\right) - \phi\left.\frac{\partial \rho_f}{\partial t}\right|_{p=\text{const}}, \quad (3)$$

where $\boldsymbol{\phi}$ is porosity, β_f is fluid compressibility, β_r is rock compressibility, and ρ_r is rock density. The energy conservation equation is used:

$$\left((1-\phi)\rho_r c_{pr} + \phi\rho_f c_{pf}\right)\frac{\partial T}{\partial t} = \nabla\cdot(K\nabla T) - \nabla\cdot\left(\mathbf{v}\rho_f h_f\right), \quad (4)$$

where ρ_r is rock density, c_{pr} is rock specific heat capacity, c_{pf} is fluid specific heat capacity, K is thermal conductivity, and h_f is the fluid's specific enthalpy. We assume instantaneous thermal equilibration between the rock and fluid.

This system of equations can be decomposed into a parabolic (diffusive) and a hyperbolic (advective) part, solved sequentially using an operator splitting technique, described in Coumou et al. 2006 and Yapparova et al. 2014. We make use of the Complex Systems Modeling Platform, CSMP++ [Matthai et al. 2007], and a hybrid finite element-finite volume scheme [Geiger et al. 2004]. This scheme solves the diffusion equations using the FE method (FEM), which is well-suited for parabolic equations, while advection is computed with the FV method (FVM), that is locally conservative and well suited for hyperbolic problems [Baliga and Patankar 1980; Cordes and Kinzelbach 1992; Coumou 2008]. Additionally, the diffusive part of the transport equations (3) and (4) is decoupled and solved separately. The solution sequence is as follows:

1. The temperature diffusion equation is solved using the FEM,
2. Heat transfer advection equations are solved using the FVM,
3. Fluid properties are updated,
4. The pressure diffusion equation is solved using the FEM,
5. New Darcy velocities are calculated.

All fluid properties are calculated as a function of temperature and pressure using the IAPS-84 equation of state for pure water [Haar, Gallagher, and Kell 1984].

3 Model Setup

The simulation domain presented here is inspired by the geological setting of Soultz-sous-Fore□ts, in which fractured but otherwise low permeability/porosity crystalline basement rock lies beneath a thick sedimentary cover [Baria et al. 1999; Bächler, Kohl, and Rybach 2003]. The geothermal gradient observed in multiple wells drilled through these units is greatly reduced in the upper portion of the basement rock, attributed to fluid convection in faults and fractures in the otherwise impermeable host.

Along these lines, we similarly divide our model into 3 layers: the top representing an impermeable cover sequence at 0.0 – 1.5 km depth, the middle representing permeable or impermeable rock with the fracture occupying the vertical interval from 1.5 – 2.5 km depth, and the bottom layer representing impermeable basement rocks below 2.5 km depth. We examine a box-shaped domain with a horizontal extent of 5 km by 5 km and 4 km thick that contains a single vertical fracture completely enclosed in its interior, with a height of 1 km and length of 2 km. Fractures in massive granitic host rocks are generally elliptical when unbound by bedding layers or other geological structures [Pollard and Aydin 1988; Zhang and Einstein 2010]. The geometric setup is strongly simplified compared to actual geologic situations with complex fracture networks (e.g., at Soultz-sous-Fore□ts, [Dezayes et al. 2011; Baillieux, Schill, and Dezayes 2011]), but was chosen in order to cleanly extract first order behavior that is undisturbed by site-specific geologic complexity. Furthermore, the simulation assumes that the fracture is instantaneously formed and filled with water, as simulating fracture growth is beyond the scope of this study. The top of the domain represents the earth's surface and has a fixed temperature of 10 °C and fixed pressure of 0.1 MPa. The bottom boundary has a prescribed heat flux of 85 mW/m^2 but is closed to fluid flow. The sides are no-flow boundaries with regards to both fluid and heat. Starting from a purely conductive steady state, we simulate transient fluid convection to 15,000 years.

To avoid superposition of the effect of convection in the fracture and thermal conductivity variations, the thermal properties of all layers are set to be identical. Furthermore, the top and bottom rock properties are the same in each model, while

the middle layer's permeability and porosity are varied from model to model, see **Table 1**. The elliptical fracture is 2 km long and 1 km tall (1000m and 500m principal radii) and placed in the middle of the middle layer, spanning the height of the middle layer but not extending into the top or bottom layers.

We simulate both narrow, open, parallel-plate fractures and wide, permeable fracture zones or faults (generically referred to as fractures for the remainder of this manuscript). Discretely modeling high aspect-ratio fractures in a large domain is accomplished by using lower-dimensional (surface) elements to represent fractures. This saves computation time while no accuracy is lost [Juanes, Samper, and Molinero 2002], but can only be used when fracture permeability is larger than host rock permeability and the fracture/fault has a large aspect ratio [Grillo et al. 1999; Kim and Deo 2000]. To describe and compare fractures of varying width and permeability, we use fracture transmissivity:

$$T_{fr} = k \cdot a \,, \tag{5}$$

where a is strictly the thickness of the permeable fracture zone. In the case of a parallel plate fracture, a represents the aperture of the open slot. It should be noted that this definition has units of length cubed and is not to be confused with hydraulic transmissivity [Jaeger, Cook, and Zimmerman 2009; McClure and Horne 2014]. Though it is unrealistic that an open fracture would exist on the scale presented here, we include it in this study, demonstrating that convection patterns and subsequent thermal anomalies are similar in both open fractures and filled fracture zones. The more realistic, wider fracture zones or faults are modeled using either lower-dimensional (2D) or volumetric (3D) elements.

To assess whether water in the host rock in each model should spontaneously convect, the dimensionless Rayleigh number of the permeable middle layer is calculated. This Rayleigh number is a dimensionless number which compares buoyancy to viscous forces and is often used to assess the onset and strength of convection [Lapwood 1948; Murphy 1979; Lowell 1975]. It is calculated as,

$$Ra = \frac{\rho_f^2 g \alpha_f H^2 k G c_{pf}}{\mu_f K_r} \,, \tag{6}$$

where α_f is thermal expansivity of water, H is the height of the rock unit, G is the geothermal gradient, K_r is the thermal conductivity of the host rock, and c_{pf} is the heat capacity of water. In general, natural convection spontaneously develops when Ra exceeds a certain critical value. This Rayleigh number definition assumes constant thermal α_f and c_{pf} resulting in a linear density variation with temperature. For a horizontal, homogeneous rock unit with a constant heat flux boundary condition at the bottom, and water properties taken at 25 °C this critical Rayleigh number is ~27.1 [Lapwood 1948; Nield 1968]. Jupp and Schultz [2000; 2004] pointed out that a

standard Rayleigh analysis may fail in the case of strong temperature and pressure dependence of fluid properties. Although our simulations use such fully temperature- and pressure-dependent water properties, the limited temperature range allows the linear Rayleigh analysis to be applied as an approximation estimating the likelihood of natural convection. As seen in **Table 1** and in agreement with our simulations, *Ra* exceeds ~27.1 and Rayleigh convection is indicated only for Model 3.

A Rayleigh number can also be calculated for fractures and faults [Murphy 1979; Tournier, Genthon, and Rabinowicz 2000], but is of minor relevance for analysis of the long-term thermal effects that we study here. Rather, as we will demonstrate, fracture transmissivity appears to be the main control on the thermal effect of convection in fracture zones. No initial thermal perturbation is required to initiate convection in our models: the use of unstructured meshes of first-order finite elements results in minute differences in fluid flow within the fracture which triggers convection, should the fracture be sufficiently permeable. Consequently, convection patterns in the fracture vary slightly between discretizations. For instance, the location of an upflow zone may be shifted from one discretization to the next, or convection cells may be slightly wider/narrower.

To compare the thermal effect of convection in a fracture, the overall additional heat flow is calculated by integrating the conductive heat flux over a horizontal slice through the whole domain, 100 m above the fracture, then subtracting the integrated background basal heat flux. To illustrate the effects of different spatial discretizations, Figure 1 shows the additional heat flow due to convection from ten different mesh realizations (each with ca. 1,000 fracture elements) for fractures with transmissivity $2.9 \cdot 10^{-11}$ m^3 and $8.3 \cdot 10^{-11}$ m^3. Lower transmissivity fractures result in fewer convection cells, making any change in cell location/width more impactful, leading to slightly larger variations between discretizations (ca. ±11% in peak additional heat flow, compared to ±6% for the higher transmissivity case). Similar results, both in magnitude and variability, are also seen in finer discretizations (ca. 2,500 fracture elements, not shown). Additionally, we investigated the effect of different mesh resolutions in the host rock walls perpendicular to fracture, which result in only minor changes and ~3% change in maximum additional heat flow.

4 Results

We first investigate the heat transport effects of fracture convection in an impermeable host, focusing on the extent of thermal perturbation and increased vertical heat transport (Model 1). Next, the host is made permeable and we investigate the secondary, non-Rayleigh fluid flow induced by convection in the fracture (Model 2). Host rock permeability is further increased to allow spontaneous Rayleigh convection in the permeable layer, altering fracture convection patterns (Model 3).

4.1 Convection in fracture zones as a function of thickness

In order to test the sensitivity of convection patterns and resulting thermal perturbations to fracture zones thickness, we simulated open, parallel-plate fractures as lower-dimensional elements (2D) as well as full-dimensional elements (3D) to model filled fracture zones. We compare convection in the fractures by keeping fracture transmissivity (i.e. permeability times thickness) constant while varying thickness. Each model uses a common mesh along the centerline of the fracture, maintaining node locations at the middle of the fracture in order to minimize mesh-related variability.

Table 2 shows the fracture properties for various fracture thicknesses, along with the resulting thermal gradient and Darcy velocity due to convection. All results shown are taken after 10,000 years of simulation time using an identical mesh of Model 1. Four models of varying thickness are shown for two values of transmissivity: $2.9 \cdot 10^{-11}$ m^3 and $8.3 \cdot 10^{-11}$ m^3, corresponding to an open slot fracture of 0.7 mm and 1.0 mm, respectively. Despite several orders of magnitude difference in thickness and permeability, the thermal effect of each of these fractures is similar. The additional heat flow through these fractures is shown in **Figure 2**. For each value of transmissivity, convection patterns, geothermal gradient inside the fracture, and additional heat flow are similar, implying that transmissivity is the primary control.

4.2 Fracture convection in impermeable host rock

There are three convective flow regimes for a large, vertical fracture: no convection, steady convection, and unsteady convection [López and Smith 1995]. Below a certain threshold permeability, the fluid flows too slowly to advect significant amounts of heat before it diffuses into the host; convection does not occur. Just above this threshold, advection begins to dominate over diffusion, resulting in the formation of convection cells, which reach a nearly steady state, changing little over time. As permeability increases, another threshold is reached and convection becomes unsteady - episodic, with some regions within the fracture never reaching a steady state. This unsteady convection is typically limited to the lateral edges of the fracture and induces only minor changes in heat transfer with the host.

When the host rock is impermeable, convection within the fracture is essentially a closed-loop system, where upward flow of water must be balanced by downward flow. Increasing fracture permeability results in larger rates of fluid flow and convective heat transfer, as well as narrower and more numerous convection cells. The circulating fracture fluid thus exchanges heat between the top and bottom of the fracture, reducing the temperature range within the fracture.

The transition between steady and unsteady convection lies between a transmissivity of $2.9 \cdot 10^{-11}$ m^3 and $4.3 \cdot 10^{-11}$ m^3. **Table 3** shows the convection regime, thermal gradient, and Darcy velocity for various fractures. This transition, however, does not affect the thermal structure of the system, as both steady and unsteady convection significantly impact the thermal gradient.

The thermal perturbation spreads into the host rock exclusively via conduction, as upward flowing, hot water heats the rock above the fracture and downward-flowing water cools the rock below**.** The extent of the perturbation around a fracture is shown for low-transmissivity ($T_{fr} = 1.04 \cdot 10^{-11}$ m^3), medium-transmissivity ($T_{fr} = 2.9 \cdot 10^{-11}$ m^3), and high-transmissivity ($T_{fr} = 8.3 \cdot 10^{-11}$ m^3) after 15,000 years simulation time is shown in **Figure 3**. The initial (conduction only) temperature of the fracture is ~74 °C at the top, 95 °C at the middle, ~116 °C at the bottom.

The strongest thermal perturbations in the host rock occur near the top (heating) and bottom (cooling) of the fracture. Less permeable fractures with only a few convection cells develop asymmetric host rock heating patterns near the top of up-flow zones that affect only rather small volumes. For example, a low-transmissivity fracture develops a +/-2 °C anomaly up to ~150 m away from the fracture. Increasing fracture transmissivity creates more numerous and narrower convection cells, which result in more symmetric and extensive heating around the upper tip of the fracture. The same is true for the cooling zone that develops surrounding the bottom perimeter of the fracture. The high-transmissivity fracture, by contrast, has a +/-2 °C anomaly which propagates up to ~400m (i.e., just less than half of the fracture height) into the host rock and the regions of strongest thermal perturbation shift upwards (heating) and downwards (cooling) in the fracture. As the thermal perturbation diffuses outward from the top of the fracture it becomes less pronounced, to the degree that the near-surface expression of such an anomaly is negligible.

The thermal perturbation is weakest in the middle depths of the fracture. At this level, contrary to the thermal effects near the top and bottom parts, fewer and wider convection cells result in wider thermal perturbations, with the +/-2 °C anomaly propagating up to 200 m into the host rock for a low-transmissivity fracture. Narrower convection cells imply a closer spacing of hot and cold regions, leading to a thermal cancellation effect away from the fracture and limiting the +/-2 °C anomaly to an approximate distance of 50 m in the high-transmissivity case. In general, given the semi-circular shape of the individual anomalies around up-/down-flow zones, this distance is limited by and roughly equal to the half width of upflow or down-flow zones inside the fracture.

4.3 Fracture convection in permeable rock

4.3.1 Fracture convection in non-convecting host rock

Fracture convection in permeable rock results in fluid flow around and into/out of the fracture itself. Model 2 features a 1000-m, moderately permeable (10^{-14} m^2) rock unit containing the fracture, bounded above and below by impermeable (10^{-18} m^2) rock (properties given in Table 1). Although thick and permeable, the Rayleigh number for this unit is ~20, less than the critical value (~27.1), and therefore fluid in the host rock does not spontaneously undergo Rayleigh-Bernard convection.

As thermal anomalies resulting from convection in the fracture propagate into the host rock, fluid near the fracture begins to flow upward and downward, as well as into and out of the fracture. The host rock permeability allows for fluid exchange with the fracture; fracture convection is no longer a closed-loop. As a result, the flow rates inside the fracture are slightly decreased (~5%) and convection cells are slightly narrowed (~10%) as rock permeability is increased from an essentially impermeable 10^{-18} m^2 to 10^{-14} m^2. Although fluid exchange between the rock and the fracture generally increases heat transfer, Darcy velocities in the host rock remain low (ca. 10^{-10} m s^{-1}, or 0.3 cm per year) and diminish away from the fracture. Therefore, the thermal impact of the fracture convection remains spatially restricted just as in the impermeable host rock scenario.

Flows into, out of, and around the fracture display a limited range of characteristic patterns as a function of host rock permeability (**Figure 4)**. Nearly all fluid exchange occurs through the fracture walls rather than through the narrow edges of the fracture.

Large, wide convection cells in the fracture, such as in the low-transmissivity case, results in a portion of the fluid flowing out of the fracture at the top of upward-flowing regions and the bottom of downward-flowing regions, where fluid flow reaches the boundary of the permeable fracture. Fluid enters the fracture at opposite ends of these up-flow and down-flow zones. Similar to the heat distribution in **Figure 3**, the location of inflow and outflow zones in the fracture may be asymmetric. Flow entering and exiting the fracture reaches up to $1.3 \cdot 10^4$ m^3 yr^{-1}. Streamlines show that this fluid is driven along wide, spiraling paths towards and away from the fracture. As fluid enters the fracture, it becomes entrained in the vigorous convection cell within it although it may exit again elsewhere. Narrower convection cells in more permeable fracture models result in fluid leaving the fracture at the upper and lower termination while entering near its middle depth. Fracture-matrix fluid exchange increases with fracture permeability, with flow into/out of the high-transmissivity fracture reaching $2.4 \cdot 10^4$ m^3 yr^{-1}, double that of the low-transmissivity fracture.

Induced host rock convection cells circulate fluid around an axis parallel to fracture strike in the more permeable fractures, i.e. the medium- and high-transmissivity cases. These form exclusively near the top of up-flow zones and at the bottom of down-flow zones, as indicated by the white arrows in **Figure 4**, with fluid flowing vertically and

perpendicular to the fracture plane. Because these zones are highly localized, they do not form continuous convection "rolls," yet share a common axis of rotation. Fluid flows in tight circles near the center of these cells, while the outer part of the cell forms long arcs, flowing further from the fracture, returning at mid-depths.

4.3.2 Fracture convection in convecting host rock

In Model 3 host rock permeability is increased to 10^{-13} m^2 in the 1000-m thick fractured layer, raising the unit's Rayleigh number to ~200 and allowing natural convection in this layer. Other model properties are given in Table 1. We focus on the high-transmissivity case ($T_{fr} = 8.3 \cdot 10^{-11}$ m^3).

Convection within the fracture initiates before Rayleigh convection in the host rock, but fracture flow patterns are increasingly perturbed and eventually dominated by convection in the host rock as the simulation progresses. **Figure 5** shows temperature, inflow/outflow, and fracture convection patterns after 250 years of simulated time, when fracture convection has already been established. By 1,500 years, convection in the host rock has begun, altering the thermal field in the permeable layer and overprinting the convection patterns within the fracture (Figure 5, middle column). Here, the fracture partially acts as a focusing zone for through-flow, hosting a single convection cell with a net downward flow of fluid. The thermal influence of host rock convection is much stronger than that of the fracture alone, creating large thermal perturbations throughout the permeable layer, independent of fracture position. Convection within the fracture remains strong, however, as it focuses the fluid flow distorting the convection cells in the host rock.

The exchange between fracture and host is increased to $1.5 \cdot 10^5$ m^3 yr^{-1}, nearly an order of magnitude larger than those seen in the high-transmissivity case of Model 2 ($2.4 \cdot 10^4$ m^3 yr^{-1}), due to the increase in host permeability. Fluid flows into the top half of the fracture and back out to the host rock in the bottom half.

5 Discussion

5.1 Thermal effects of convection in a fracture

Convective fluid circulation inside a fracture cools its bottom part, increasing and focusing heat flux from the host rock to the fracture via conduction. This additional heat is then convected upwards by fluid within the fracture. At the top of the fracture, temperature increases and drives additional heat flux into the host rock, again via conduction. **Figure 6** shows this behavior in two vertical cross-sections (parallel and perpendicular to the fracture plane) of a high-transmissivity fracture in Model 1 (impermeable host) at 10,000 years.

The thermal effect of the fracture is analogous to a thin, vertical region of increased thermal conductivity. An effective thermal conductivity, K_{eff}, can be calculated:

$$K_{eff} = \frac{\left(q''_{basal} A_{frac} + q_{additional}\right)\Delta z}{A_{frac}\Delta T}, \quad (7)$$

where q''_{basal} is the basal heat flux, A_{frac} is the cross sectional area of the fracture (horizontal length times thickness), $q_{additional}$ is the additional heat flow due to fracture convection, Δz is the height of the fracture, and ΔT is the vertical temperature difference within the fracture. Convection within the fracture locally increases heat flux beyond the basal heat flow of 85 mW m^{-2}, diminishing away from the fracture.

Note that the K_{eff} computed with this convention will be maximized in the case of a parallel plate fracture, as A_{frac} is minimized for an open conduit. With the same transmissivity, a less permeable, gauge-filled fracture zone may have a much larger width, increasing A_{frac}. The resulting K_{eff} would be significantly smaller than the parallel plate fracture. **Table 4** shows the effective thermal conductivities obtained for the different parallel plate aperture values given in Table 1. As aperture increases, temperature difference decreases while K_{eff} increases.

Figure 7 shows the additional heat flow due to fracture convection over time, measured at a plane 100 m above the fracture. When convection initiates inside the fracture, the heat flow increases, then peaks, and subsequently decreases slowly as the fracture's heat source depletes. For a fracture transmissivity of $8.3 \cdot 10^{-8}$ m^3, the largest fracture simulated here, the local heat flux above the fracture reaches a maximum of ca. 315 mW m^{-2} (ca. 4 times the background heat flux), while a $8.33 \cdot 10^{-11}$ m^3 fracture (high-transmissivity case) increases heat flux up to ca. 215 mW m^{-2} (ca. 2.5 times the background heat flux). Due to the diffusive propagation of the thermal perturbation, the maximum heat flux decreases further above the fracture.

The conductive heat source at the bottom of the fracture is initially strong, as temperature gradients are steep. Progressive cooling of the rock over time reduces the thermal gradient and, accordingly, the heat supplied to the fracture fluid for convection. For each unique fracture transmissivity, the maximum heat flux occurs at a different time, determined by the time it takes for convection to initiate and the development of the thermal perturbation in the host rock. Notably, convection initiates well within the range of the "delayed neutral stability" regime defined by Murphy 1979.

Figure 8 shows the additional heat flux as a function of fracture transmissivity. Again, the three regimes are present: no convection when transmissivity is below $5.3 \cdot 10^{-12}$ m^3, onset of convection with quickly increasing thermal effect up to $6.7 \cdot 10^{-10}$

m^3 (equivalent to a 2-mm parallel plate aperture) and plateau of thermal effect above this, i.e. a maximum of possible heat flow focusing is reached.

5.2 Importance of transmissivity in fracture convection patterns

Previous studies [Murphy 1979] used a modified Rayleigh number to assess characteristics of convection in thin faults and fractures, replacing *H* with *a* in equation (6) to account for the importance of fracture aperture:

$$Ra^* = \frac{\rho_f^2 g \alpha_f a^2 k G c_{pf}}{\mu_f K_r} \ , \qquad (7)$$

Thus, the critical Rayleigh number varies with a^2k for fracture convection. Using this criterion, only extremely permeable fractures (parallel plate aperture over ca. 0.1 m, T_{fr} over ca. 10^{-4} m^3) would develop convection. However, Murphy [1979] and Tournier et al. [2000] also posit that the critical Rayleigh number for these systems decreases with time, allowing non-spontaneously convecting fractures to develop convection after an "incubation" period, which varies with $(ak)^2$, or T_{fr}^2. Using a time-varying Rayleigh number to determine fracture convection behavior leads to ambiguous comparisons. Additionally, the existence, incubation time, and thermal effect of this delayed fracture convection are not well correlated with the fracture Rayleigh number. This is shown in **Table 5** for the models presented in **Table 2** and **Figure 2**. The critical Rayleigh number calculated for these models using equation (7) varies by 4 orders of magnitude for each value of transmissivity, despite similar convection patterns and thermal effects.

As **Table 2** and **Figure 2** together show, fracture transmissivity, the product of thickness and permeability, is the primary controlling factor in fracture convection patterns and resulting thermal perturbations. For a given transmissivity, convection incubation time and additional heat flow are similar (**Figure 2**), as well as the resulting geothermal gradient through the fracture (**Table 5**). This single parameter therefore appears to be a more appropriate metric, as it allows for useful comparisons between fractures of varying thickness, whereas critical Rayleigh number may vary by several orders of magnitude.

5.3 Interaction between convection in a fracture and flow in the permeable host rock

While an increase in permeability from an essentially impermeable 10^{-18} m^2 to a moderately permeable 10^{-14} m^2 host rock had only a moderate effect on the thermal perturbations, the increase in permeability from 10^{-14} m^2 to 10^{-13} m^2 significantly

affected fluid flow and thermal patterns in and around the fracture. This transition correlates with the critical Rayleigh number for porous medium convection.

The moderately permeable host rock in Model 2 has a Raleigh number below the critical value and therefore does not spontaneously convect, but nonetheless facilitates secondary convection near the fracture. Thermal perturbations created by spontaneous convection within the fracture induce lateral temperature variations in the host rock. Host fluid is heated near hot up-flow zones in the fracture and is buoyantly driven upward; down-flow zones in the fracture cause host fluid to cool and sink. Thus, secondary convection in the host rock mimics the patterns within the fracture, while fluid exchange with the fracture drives flow perpendicular to the fracture plane. The resulting host rock flow patterns are complex and depend on convection cell size within the fracture. When fracture permeability is high, fluid may begin to circulate about an axis of rotation perpendicular to the convection cells within the fracture. This secondary, subcritical convection is relatively weak and thermally insignificant, with Darcy velocities reaching $3.1 \cdot 10^{-9}$ m s^{-1} and quickly diminishing away from the fracture, having no effect on convection patterns within the fracture.

Fluid exchange between fracture and host rock are shown to increase with fracture aperture and transmissivity. Because the fracture and permeable layer are confined by the impermeable rock units above and below, fluid entering the fracture flows back to this permeable layer, though at a different location. Thus our results are in agreement with the result from López and Smith [1995; 1996], despite their model permitting the discharge of fluid from the fracture to the surface, and show that a convecting fracture plays an important role in reservoir fluid circulation regardless of surface expression or hydraulic connection.

When host rock permeability is increased in Model 3 and Rayleigh number exceeds the critical value, convection in the host rock becomes the dominant force in the system, with Darcy velocities reaching $2.6 \cdot 10^{-8}$ m s^{-1}. Although convection within the fracture is initiated first, convection in the host dictates the flow patterns in the fracture, overprinting the fracture's established patterns and thermal perturbation. Depending on the relative sizes of the fracture and convection cells, a fracture may serve as a unidirectional conduit for fluid flow or as a focal point for circulation. Using the models presented here, the fluid flow in the fracture tended to flow in a single convection cell.

5.4 Relevance to natural systems and applications

The thermal anomalies seen above the convecting fracture and the alteration of the geothermal gradient in and near the fracture appear similar to the patterns observed at Soultz-sous-Fore□ts, albeit with a weaker thermal perturbation than observed in the field, as only a single fracture is modeled here. Our results add another perspective to

the understanding of thermal anomalies in the Rhine Graben, for which the exact generating mechanisms are a matter on ongoing debate [Guillou-Frottier et al. 2013; Bächler, Kohl, and Rybach 2003]. They indicate that further study is needed of convection patterns in large, realistic fracture/fault networks and the resultant thermal anomalies surrounding them. Such studies will aid in better defining the potential of geothermal exploration targets. Targets for Enhanced Geothermal Systems (EGS) are often in deep, fractured crystalline basement below the sedimentary cover and pre-drilling assessment of their thermo-hydraulic properties has remained intrinsically difficult.

Further work is needed to understand the thermal impact of different geometries, such as smaller, less extensive fractures or inclined fractures. Additionally, convection patterns and strength may be significantly impacted by spatial and temporal transmissivity variations, such as fracture heterogeneity [López and Smith 1996], mechanical fracture creation/contraction/dilation (including thermo-mechanical and hydro-mechanical effects)[Barton, Bandis, and Bakhtar 1985], and chemical precipitation/dissolution [Berkowitz 2002; Taron and Elsworth 2009].

Fluid convection in large fractures is a key process in the formation of hydrothermal vein-type deposits. The shape of convection cells and fluid mixing have been considered major controls on the spatial variation of the ore grade of such veins. For example, the interaction between convection in the fracture and its interaction with convection in permeable host rocks has been inferred from careful ore grade mapping at Topia, Durango, Mexico [Loucks and Petersen 1988]. Like López and Smith [1995], we've shown that convection promotes fluid mixing with the host rock. Additionally, our results provide the first – although still generic – simulation evidence that convection cell shape and size, as well as fracture transmissivity, control the location for such mixing.

6 Conclusions

Convection within a fracture or fault zone focuses the heat flow from the surrounding rocks and transports the heat upwards via convection. The degree of this focusing is highly sensitive to transmissivity up to a certain value, above which the heat flux reaches a plateau determined by fracture geometry. In the simulations presented here, convection within the 2 x 1-km fracture added nearly 60 kW to the purely conductive heat flux and perturbed the temperature up to 500 m away. The strength of the thermal perturbations is primarily controlled by fracture geometry while their location is controlled by convection cell width: wide cells maximize perturbations at intermediate depth in the convecting layer; narrow cells maximize them at the top and bottom of the fracture.

We show that flow patterns in the host rock surrounding the fracture are highly dependent on and linked with the up-flow and down-flow zones that develop within

the fracture. Fluid exchange between fracture and host rock are dependent on the arrangement and size of convection cells. Large convection cells induce wave-like regions of flow into and out of the fracture, while narrow cells result in horizontal bands of inflow and outflow. Additionally, we have shown that secondary (lateral thermal gradient induced) convection cells can form in the host rock itself, with fluid circulating around an axis parallel to fracture strike. This subcritical convection in the host rock has little to no thermal impact or effect on convection patterns within the fracture. However, beyond a critical rock permeability, natural convection will dominate and overprint the flow patterns within the fracture. The fracture becomes a part of the overall convection pattern in the host, focusing flow and heat transport. Although we simulated a much simplified fracture geometry, our results indicate that simulations with explicitly represented fractures may provide key insights, explaining the links between field observations from geothermal and mineral deposits and the dynamics of buoyancy-driven fluid flow.

We hope that the results and methods employed in this study may prove helpful in site selection of geothermal reservoirs, both for EGS in basement rock and within overlying conventional reservoirs. The results aid in understanding of how natural convection may be exploited to mine heat more effectively from such systems in the future.

Acknowledgements
We acknowledge funding by the Swiss National Research Program NRP70 “Energy Turnaround”, grant number 407040L_153971 (“Modelling permeability and stimulation for deep heat mining”) and grant number 200020_172851 (“Key problems of heat and mass transfer in the Earth’s crust”). The constructive inputs of Dina López, an anonymous reviewer, and associate editor André Revil helped to significantly sharpen the ideas presented in this paper. The data presented in this study are available at: https://doi.org/10.3929/ethz-b-000242678

Table 1: Rock properties

Region	Φ	ρ_r [kg m^{-3}]	c_{pr} [J kg^{-1} K^{-1}]	K_r [W m^{-1} K^{-1}]	k [m^2]	Ra[(a)]	*Natural convection in host rock*
Top/Bottom	0.03	2650	800	2	10^{-18}	~$2 \cdot 10^{-3}$	No
Middle (Model 1)	0.03	2650	800	2	10^{-18}	~$2 \cdot 10^{-3}$	No
Middle (Model 2)	0.10	2650	800	2	10^{-14}	~$2 \cdot 10^{1}$	No
Middle (Model 3)	0.10	2650	800	2	10^{-13}	~$2 \cdot 10^{2}$	Yes
Fracture	1.00	-	-	-	variable	variable	Yes

(a) Parameters values used in the calculation of Ra are g = 9.81 m s^{-2}, α_f = $6.5 \cdot 10^{-4}$ K^{-1}, c_{pf} = $4.2 \cdot 10^{3}$ J K^{-1}, μ_f = $3 \cdot 10^{-4}$ Pa s^{-1}. True values of fluid properties used in the simulations vary as a function of temperature and pressure, i.e., these values are approximations.

Table 2: Effect of varying fracture thickness with constant transmissivity

Fracture Transmissivity (m^3)	Thickness (m)	Permeability (m^2)	$\Delta T^{(a)}$ (°C)	Max Darcy Velocity (m/s)
$2.9 \cdot 10^{-11}$	$0.7 \cdot 10^{-3}$	$4.1 \cdot 10^{-8}$	32.5	$5.8 \cdot 10^{-3}$
$2.9 \cdot 10^{-11}$	1.0	$2.9 \cdot 10^{-11}$	32.3	$4.0 \cdot 10^{-6}$
$2.9 \cdot 10^{-11}$	3.0	$9.5 \cdot 10^{-12}$	32.0	$1.3 \cdot 10^{-6}$
$2.9 \cdot 10^{-11}$	10.0	$2.9 \cdot 10^{-12}$	31.6	$3.8 \cdot 10^{-7}$
$8.3 \cdot 10^{-11}$	$1.0 \cdot 10^{-3}$	$8.3 \cdot 10^{-8}$	22.5	$8.1 \cdot 10^{-3}$
$8.3 \cdot 10^{-11}$	1.0	$8.3 \cdot 10^{-11}$	22.0	$7.8 \cdot 10^{-6}$
$8.3 \cdot 10^{-11}$	3.0	$2.8 \cdot 10^{-11}$	22.2	$2.5 \cdot 10^{-6}$
$8.3 \cdot 10^{-11}$	10.0	$8.3 \cdot 10^{-12}$	22.4	$8.1 \cdot 10^{-7}$

(a) ΔT is the temperature difference between the upper and low tip of the fracture.

Table 3: Effect of fracture aperture / transmissivity on convection.

Fracture Transmissivity (m^3)	Parallel Plate Aperture (mm)	Convection Type	Number of Convection Cells	$\Delta T^{(a)}$ (°C)	Max Darcy Velocity (m/s)
0.0	0.0	None	-	42.50	-
$2.3 \cdot 10^{-12}$	0.3	None	-	42.39	$8.7 \cdot 10^{-5}$
$5.3 \cdot 10^{-12}$	0.4	Steady	1	42.27	$1.6 \cdot 10^{-4}$
$1.0 \cdot 10^{-11}$	0.5	Steady	1.5-2	40.71	$1.4 \cdot 10^{-3}$
$2.9 \cdot 10^{-11}$	0.7	Steady	2.5-3.5	27.23	$5.7 \cdot 10^{-3}$
$4.3 \cdot 10^{-11}$	0.8	Unsteady	3-4	23.42	$6.9 \cdot 10^{-3}$
$8.3 \cdot 10^{-11}$	1.0	Unsteady	3.5-5	17.42	$7.9 \cdot 10^{-3}$
$6.7 \cdot 10^{-10}$	2.0	Unsteady	3.5-5	4.72	$1.2 \cdot 10^{-2}$
$1.0 \cdot 10^{-8}$	5.0	Unsteady	4-5	1.31	$2.4 \cdot 10^{-2}$

All results taken after 10,000 years of simulation time using identical mesh of Model 1. [(a)] ΔT is the temperature difference between the upper and low tip of the fracture.

Table 4: Effective thermal conductivities for Model 1 (impermeable host)

Fracture Transmissivity (m^3)	Fracture Aperture (mm)	ΔT (°C)	Parallel plate K_{eff} [W m^{-1} K^{-1}]	1 m thick K_{eff} [W m^{-1} K^{-1}]
0.0	0.0	42.50	2.00	2.0
$2.3 \cdot 10^{-12}$	0.3	42.39	$1.04 \cdot 10^{3}$	2.3
$5.3 \cdot 10^{-12}$	0.4	42.27	$1.19 \cdot 10^{3}$	2.5
$1.0 \cdot 10^{-11}$	0.5	40.71	$4.14 \cdot 10^{4}$	$2.3 \cdot 10^{1}$
$2.9 \cdot 10^{-11}$	0.7	27.23	$4.25 \cdot 10^{5}$	$3.0 \cdot 10^{2}$
$4.3 \cdot 10^{-11}$	0.8	23.42	$5.20 \cdot 10^{5}$	$4.2 \cdot 10^{2}$
$8.3 \cdot 10^{-11}$	1.0	17.42	$6.43 \cdot 10^{5}$	$6.5 \cdot 10^{2}$
$6.7 \cdot 10^{-10}$	2.0	4.72	$1.28 \cdot 10^{6}$	$2.6 \cdot 10^{3}$
$1.0 \cdot 10^{-8}$	5.0	1.31	$2.69 \cdot 10^{6}$	$1.4 \cdot 10^{4}$

Table 5: Effect of varying fracture thickness with constant transmissivity

Fracture Transmissivity (m^3)	**Thickness (m)**	**Permeability (m^2)**	**Δ T (°C)[a]**	Ra^*_{frac} [b]
$2.9 \cdot 10^{-11}$	$0.7 \cdot 10^{-3}$	$4.1 \cdot 10^{-8}$	32.5	$\sim 4 \cdot 10^{-5}$
$2.9 \cdot 10^{-11}$	1.0	$2.9 \cdot 10^{-11}$	32.3	$\sim 5 \cdot 10^{-2}$
$2.9 \cdot 10^{-11}$	3.0	$9.5 \cdot 10^{-12}$	32.0	$\sim 2 \cdot 10^{-1}$
$2.9 \cdot 10^{-11}$	10.0	$2.9 \cdot 10^{-12}$	31.6	$\sim 5 \cdot 10^{-1}$
$8.3 \cdot 10^{-11}$	$1.0 \cdot 10^{-3}$	$8.3 \cdot 10^{-8}$	22.5	$\sim 1 \cdot 10^{-4}$
$8.3 \cdot 10^{-11}$	1.0	$8.3 \cdot 10^{-11}$	22.0	$\sim 1 \cdot 10^{-1}$
$8.3 \cdot 10^{-11}$	3.0	$2.8 \cdot 10^{-11}$	22.2	$\sim 4 \cdot 10^{-1}$
$8.3 \cdot 10^{-11}$	10.0	$8.3 \cdot 10^{-12}$	22.4	$\sim 1 \cdot 10^{0}$

[a] ΔT is the temperature difference between the upper and low tip of the fracture.
[b] Parameter values given in Table 1.

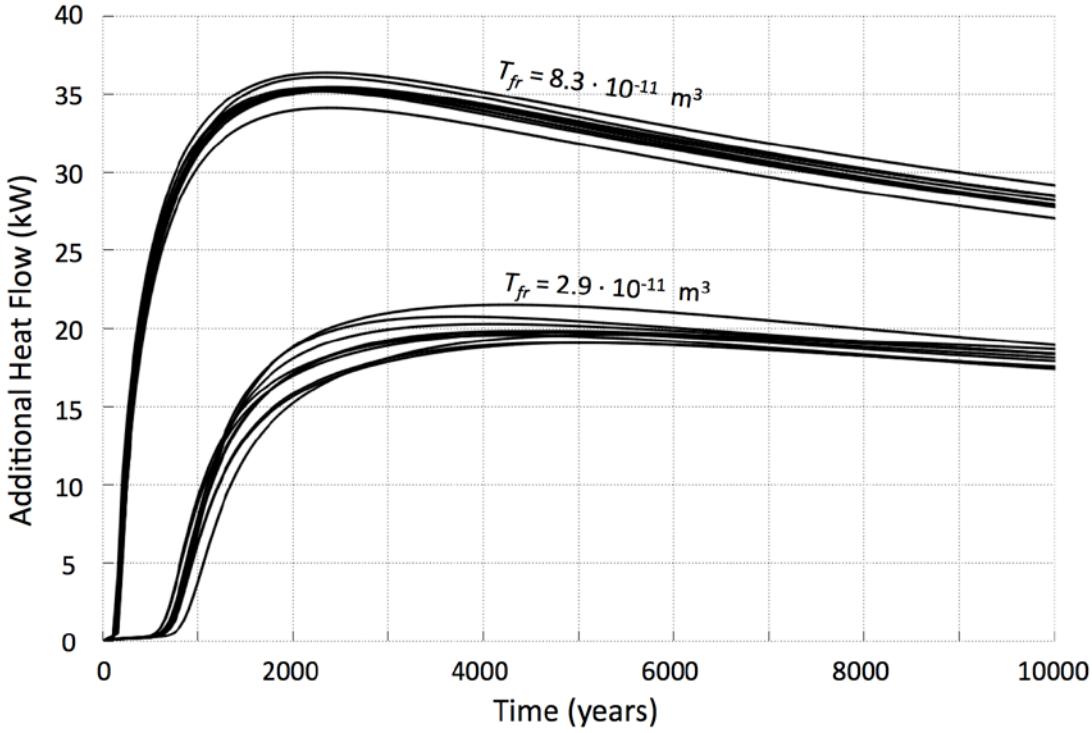

Figure 1: Variation in additional heat flow through the fracture due to different meshes. Ten realizations with roughly the same number of elements (ca. 1,000) are used to model convection in fractures with transmissivity of $2.9 \cdot 10^{-11}$ m^3 and $8.3 \cdot 10^{-11}$ m^3.

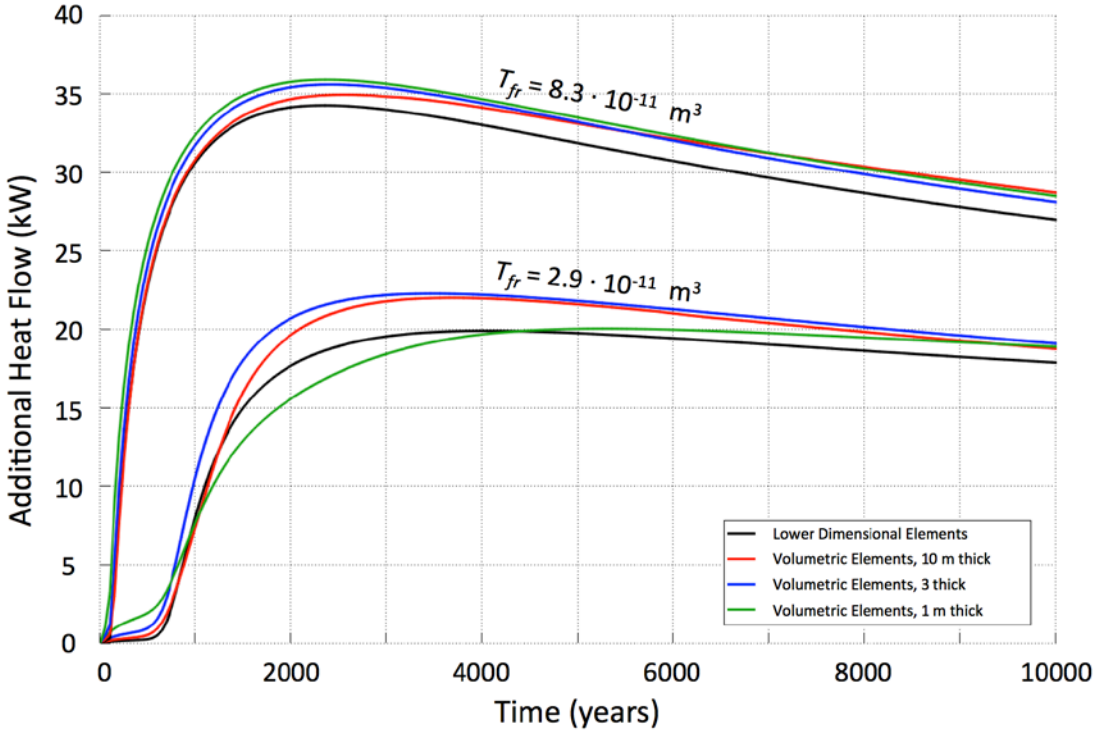

Figure 2: Comparison between lower-dimensional open slot fractures and full-dimensional filled fracture zones for two values of transmissivity.

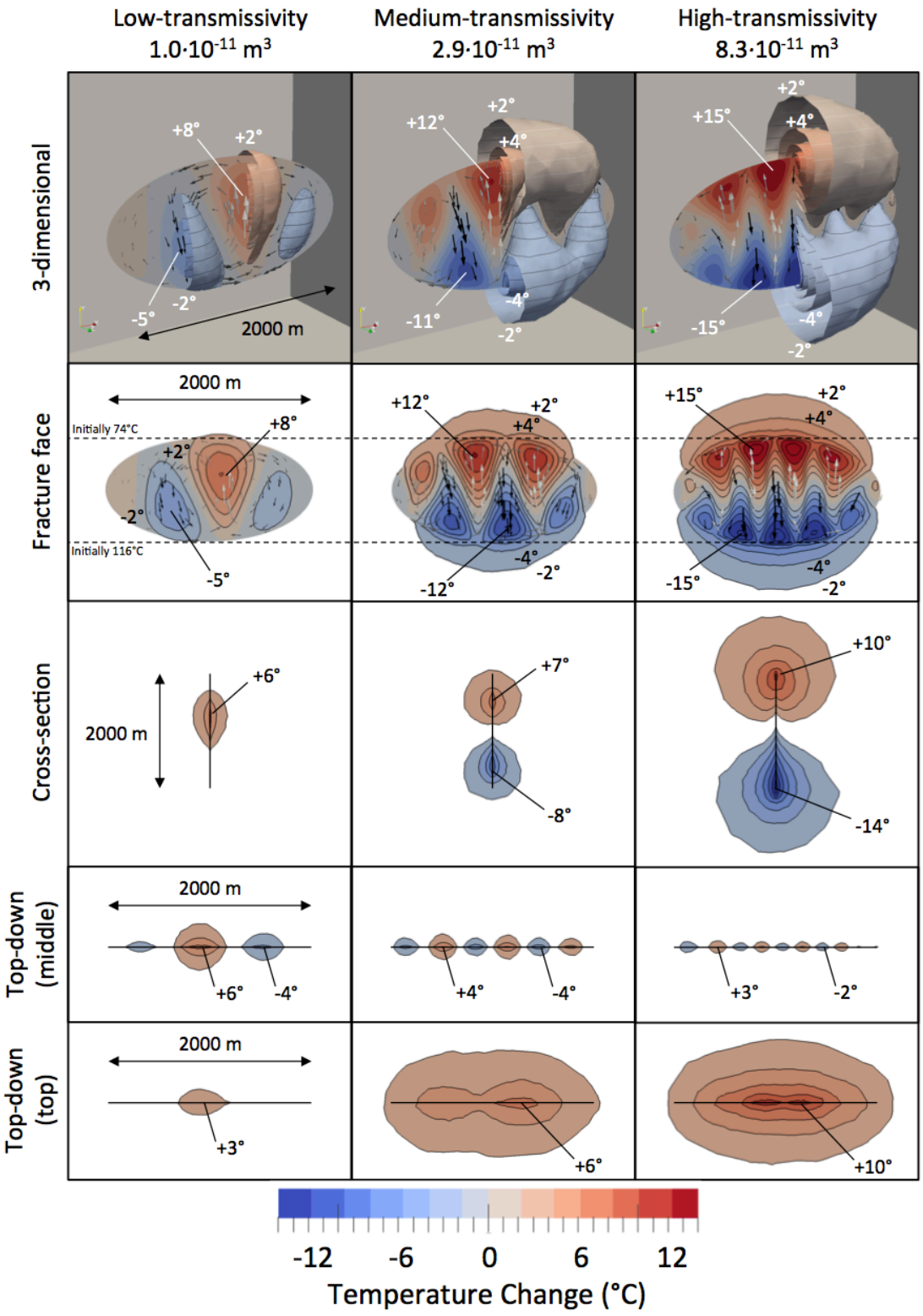

Figure 3: Temperature perturbation due to fracture convection for low-, medium-, and high-transmissivity fractures ($1.0 \cdot 10^{-11}$ m^3, $2.9 \cdot 10^{-11}$ m^3, and $8.3 \cdot 10^{-11}$ m^3, respectively). Blue indicates cooling and correspond to downward-flowing regions; red indicates heating and correspond to upward-flowing regions; contour lines and shades of blue/red each represent 2 °C change. In 3-dimensional view, contour lines on bubbles at 100m depth intervals. Snapshots taken at 15,000 years.

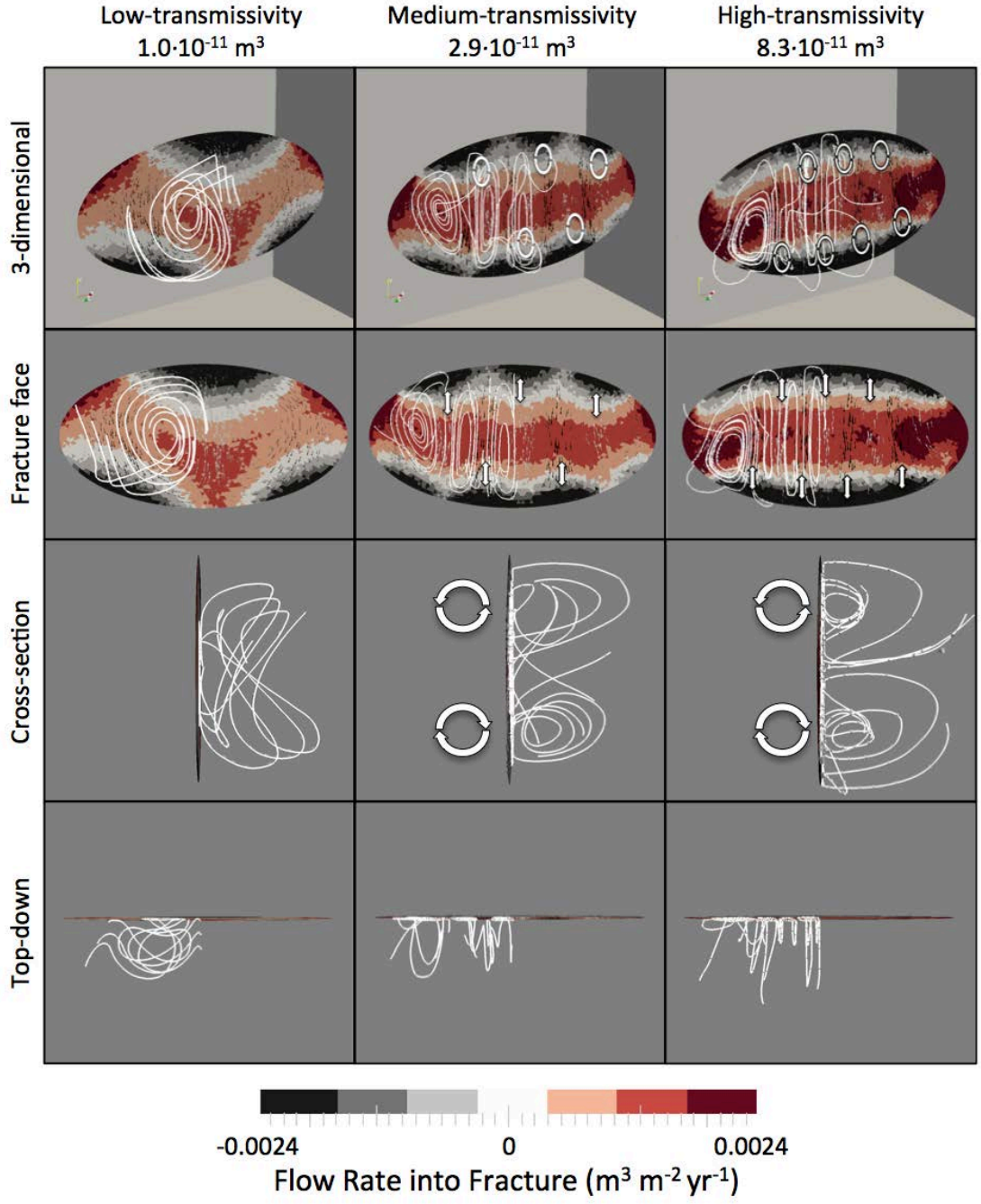

Figure 4: Flow into (red) and out of (gray/black) fracture from permeable host rock. Streamlines show complex, three-dimensional flow patterns near the fracture. Arrows in the medium- and high-transmissivity fractures indicate non-Rayleigh convection cells. Snapshots taken at 15,000 years.

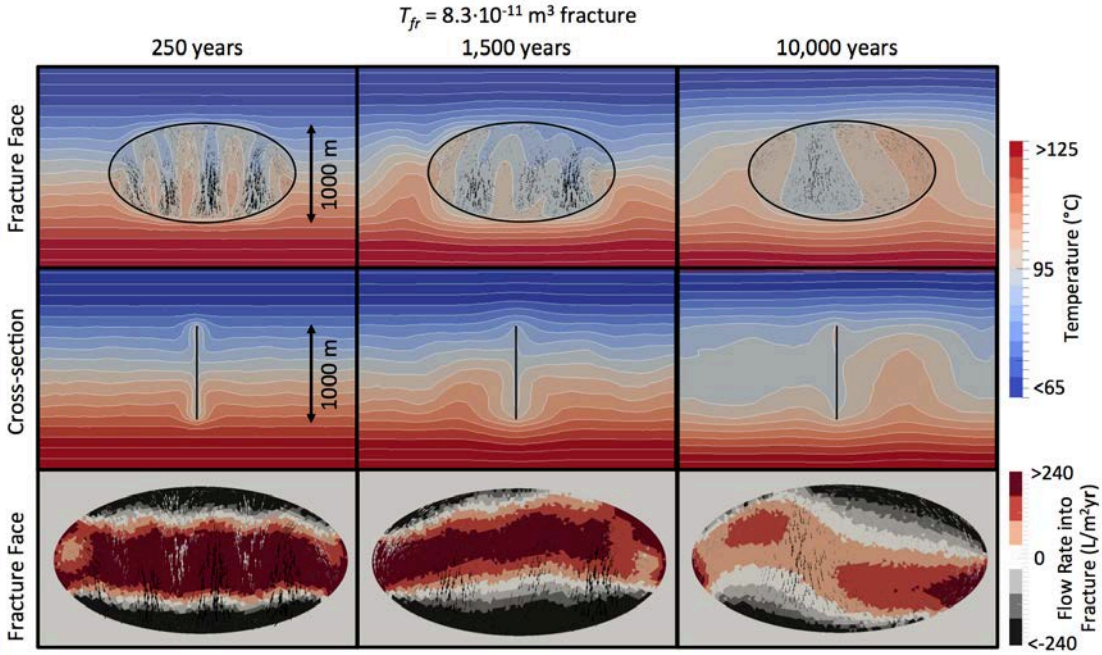

Figure 5: Fracture transmissivity is 8.3·10-11 m^3 (high-transmissivity case) and host rock permeability is 10^{-13} m^2; temperature contours drawn every 5 °C. White arrows indicate upward flow; black arrows indicate downward flow. Fracture convection develops within 250 years, but convection patterns are changed by host rock convection by 1,500 years. After 10,000 years, convection patterns in the fracture are completely dominated by host rock convection patterns and temperature.

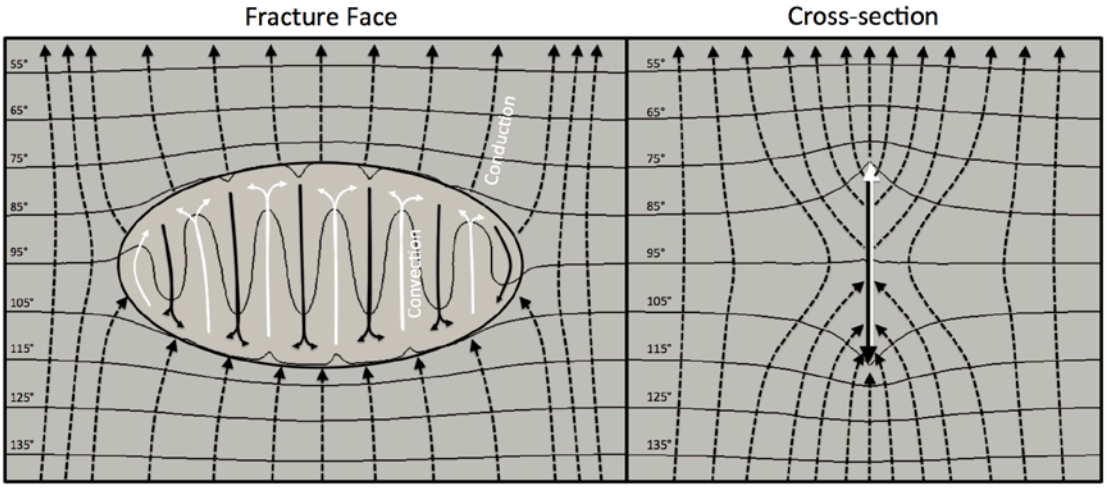

Figure 6: Interpretation of heat transfer processes around a fracture (T_{fr} = 8.3·10-11 m^3) in an impermeable host rock at 10,000 years. Temperature contours every 10 °C. Dashed arrows indicate conductive heat flow; white/black solid arrows indicate upward/downward convective flow.

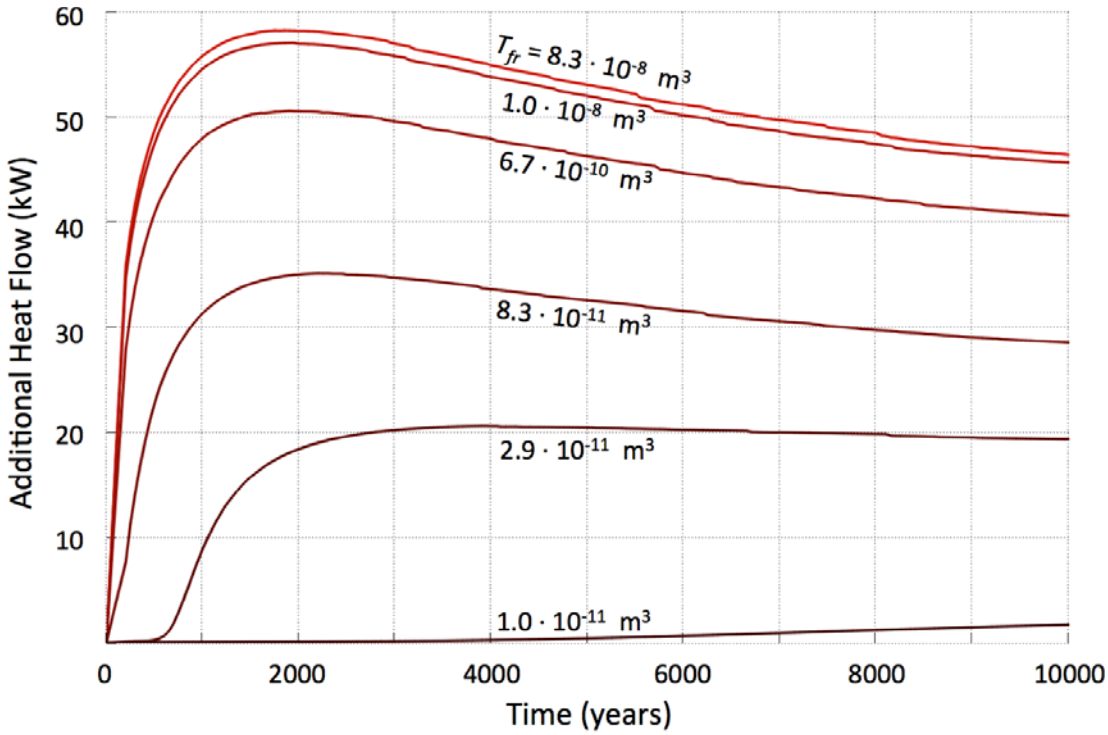

Figure 7: Additional (convective) heat flux 100-m above the fracture due to fracture convection for various values of fracture transmissivity. For the low-transmissivity case (lowest curve presented), convection takes over 10,000 years longer to initiate than for the most permeable cases; the peak heat-flow occurs after 10,000 years.

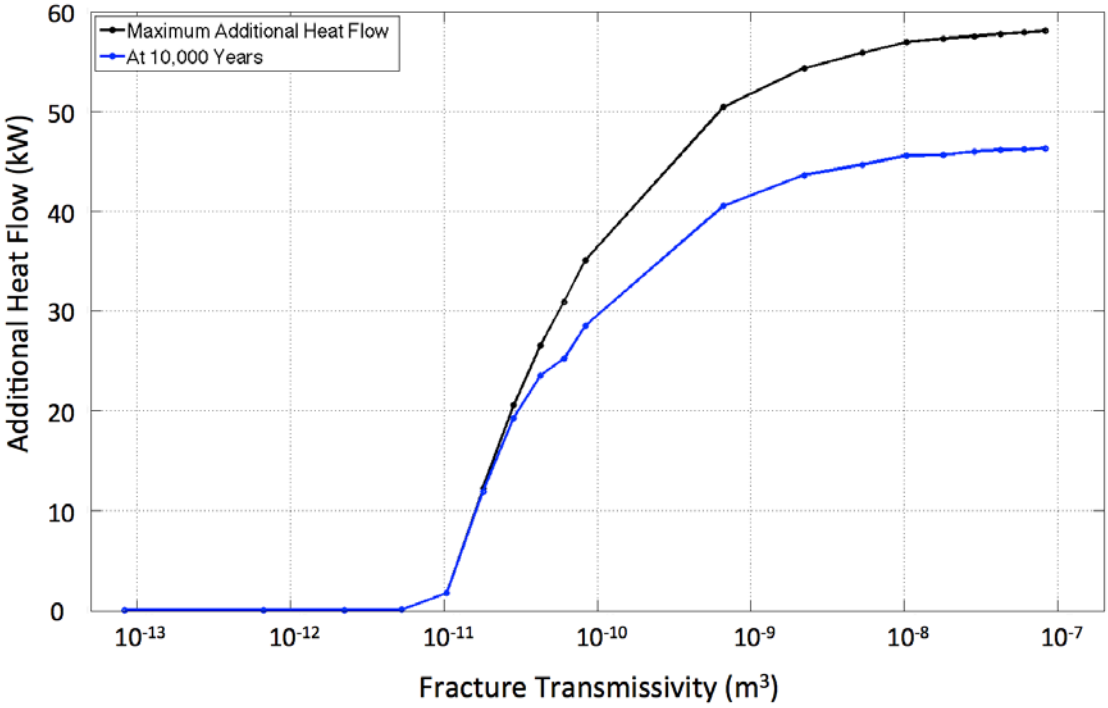

Figure 8: Additional heat flux from fracture convection as a function of fracture transmissivity. Below $5.3 \cdot 10^{-12}$ m^3, the thermal effect of fracture convection is negligible; between $5.3 \cdot 10^{-12}$ $m^3$and $6.7 \cdot 10^{-12}$ m^3, the thermal effect quickly increases; above $6.7 \cdot 10^{-12}$ m^3 the effect plateaus.

Bächler, D., T. Kohl, and L. Rybach. 2003. "Impact of Graben-Parallel Faults on Hydrothermal Convection-Rhine Graben Case Study." *Physics and Chemistry of the Earth* 28 (9–11): 431–41. doi:10.1016/S1474-7065(03)00063-9.

Baillieux, P., E. Schill, and Chrystel Dezayes. 2011. "3D Structural Regional Model of the EGS Soultz Site (Northern Upper Rhine Graben, France): Insights and Perspectives." *Proceedings of the 36th Workshop on Geothermal Reservoir Engineering*.

Baliga, B. R., and S. V. Patankar. 1980. "A New Finite-Element Formulation for Convection-Diffusion Problems." *Numerical Heat Transfer* 3 (4): 393–409. doi:10.1080/01495728008961767.

Baria, Roy, Jörg Baumgärtner, André Gérard, Jung Reinhard, and John Garnish. 1999. "European HDR Research Programme at Soultz-Sous-Forêts (France) 1987-1996." *Geothermics* 28 (4–5): 655–69. doi:10.1016/S0375-6505(99)00036-X.

Barton, N., S. Bandis, and K. Bakhtar. 1985. "Strength, Deformation and Conductivity Coupling of Rock Joints." *International Journal of Rock Mechanics and Mining Sciences* 22 (3): 121–40.

Bear, Jacob. 1972. *Dynamics of Fluids in Porous Media*. New York: Elsevier.

Berkowitz, Brian. 2002. "Characterizing Flow and Transport in Fractured Geological Media: A Review." *Advances in Water Resources* 25 (8–12): 861–84. doi:10.1016/S0309-1708(02)00042-8.

Chan, M. A., W. T. Parry, and J. R. Bowman. 2000. "Diagenetic Hematite and Manganese Oxides and Fault-Related Fluid Flow in Jurassic Sandstones, Southeastern Utah." *AAPG Bulletin* 84 (9): 1281–1310. doi:10.1306/A9673E82-1738-11D7-8645000102C1865D.

Clauser, Christoph, Erika Griesshaber, and Horst J. Neugebauer. 2002. "Decoupled Thermal and Mantle Helium Anomalies: Implications for the Transport Regime in Continental Rift Zones." *Journal of Geophysical Research* 107 (B11): 2269. doi:10.1029/2001JB000675.

Cordes, Christian, and Wolfgang Kinzelbach. 1992. "Continuous Groundwater Velocity Fields and Path Lines in Linear, Bilinear, and Trilinear Finite Elements." *Water Resources Research* 28 (11): 2903–11. doi:10.1029/92WR01686.

Coumou, Dim. 2008. "Numerical Simulation of Fluid Flow in Mid-Ocean Ridge Hydrothermal Systems." ETH Zurich. doi:10.1016/j.ijheatfluidflow.2008.05.005.

Coumou, Dim, Thomas Driesner, Sebastian Geiger, Christoph A. Heinrich, and Stephan Matthäi. 2006. "The Dynamics of Mid-Ocean Ridge Hydrothermal Systems: Splitting Plumes and Fluctuating Vent Temperatures." *Earth and Planetary Science Letters* 245 (1–2): 218–31. doi:10.1016/j.epsl.2006.02.044.

Dezayes, Chrystel, Laurent Beccaletto, Gwénolé Oliviero, Paul Baillieux, and Eva Schill. 2011. "3-D Visualization of a Fractured Geothermal Field: The Example of the EGS Soultz Site (Northern Upper Thine Graben, France)." *PROCEEDINGS, Thirty-Sixth Workshop on Geothermal Reservoir Engineering Stanford University, Stanford*.

Eichhubl, Peter, Nicholas C. Davatzes, and Stephen P. Becker. 2009. "Structural and Diagenetic Control of Fluid Migration and Cementation along the Moab Fault, Utah." *AAPG Bulletin* 93 (5): 653–81. doi:10.1306/02180908080.

Evans, Keith F., Albert Genter, and Judith Sausse. 2005. "Permeability Creation and Damage due to Massive Fluid Injections into Granite at 3.5 Km at Soultz: 1. Borehore Observations." *Journal of Geophysical Research B: Solid Earth* 110 (4): 1–14. doi:10.1029/2004JB003169.

Faulds, James, Mark Coolbaugh, Vincent Bouchot, Inga Moeck, and Kerem Oğuz. 2010. "Characterizing Structural Controls of Geothermal Reservoirs in the Great Basin, USA, and Western Turkey: Developing Successful Exploration Strategies in Extended." *Proceedings World Geothermal Congress 2010*. http://hal.archives-ouvertes.fr/hal-00495884/.

Geiger, S, S Roberts, S K Mattha, C Zoppou, and A Burri. 2004. "Combining Finite Element and

Finite Volume Methods for Efficient Multiphase Flow Simulations in Highly Heterogeneous and Structurally Complex Geologic Media." *Geofluids* 4: 284–99.
Genter, Albert, Keith Evans, Nicolas Cuenot, Daniel Fritsch, and Bernard Sanjuan. 2010. "Contribution of the Exploration of Deep Crystalline Fractured Reservoir of Soultz to the Knowledge of Enhanced Geothermal Systems (EGS)." *Comptes Rendus - Geoscience* 342 (7–8). Academie des sciences: 502–16. doi:10.1016/j.crte.2010.01.006.
Grillo, A., M. Lampe, D. Logashenko, S. Stichel, and G. Wittum. 1999. "SIMULATION OF SALINITY- AND THERMOHALINE-DRIVEN FLOW IN FRACTURED POROUS MEDIA." *Journal of Porous Media* 15 (5): 439–58.
Guillou-Frottier, Laurent, Clément Carre, Bernard Bourgine, Vincent Bouchot, and Albert Genter. 2013. "Structure of Hydrothermal Convection in the Upper Rhine Graben as Inferred from Corrected Temperature Data and Basin-Scale Numerical Models." *Journal of Volcanology and Geothermal Research* 256: 29–49. doi:10.1016/j.jvolgeores.2013.02.008.
Haar, Lester, John S. Gallagher, and George S. Kell. 1984. *NBS/NRC Steam Tables : Thermodynamic and Transport Properties and Computer Programs for Vapor and Liquid States of Water in SI Units*. Washington D.C.: Hemisphere Pub. Corp.
Haynes, D W, K C Cross, R T Bills, and M H Reed. 1995. "Olympic Dam Ore Genesis: A Fluid Mixing Model." *Economic Geology* 90: 281–307. doi:10.2113/gsecongeo.90.2.281.
Holst, P.H., and K. Aziz. 1972. "Transient Three-Dimensional Natural Convection in Confined Porous Media." *International Journal of Heat Mass Transfer* 15: 73–90.
Ingebritsen, S. E., and M. S. Appold. 2012. "The Physical Hydrogeology of Ore Deposits." *Economic Geology* 107 (4): 559–84. doi:10.2113/econgeo.107.4.559.
Ingebritsen, S. E., S. Geiger, S. Hurwitz, and T. Driesner. 2010. "Numerical Simuation of Magmatic Hydrothermal Systems." *Reviews of Geophysics*, no. 48: 1–33. doi:10.1029/2009RG000287.1.PURPOSE.
Jaeger, John Conrad, Neville G. W. Cook, and Robert Zimmerman. 2009. *Fundamentals of Rock Mechanics*. Malden, MA, USA: Blackwell Publishing.
Juanes, Ruben, Javier Samper, and Jorge Molinero. 2002. "A General and Efficient Formulation of Fractures and Boundary Conditions in the Finite Element Method." *International Journal for Numerical Methods in Engineering* 54 (12): 1751–74. doi:10.1002/nme.491.
Jupp, Tim E, and Adam Schultz. 2004. "Physical Balances in Subseafloor Hydrothermal Convection Cells." *Journal of Geophysical Research* 109: 1–12. doi:10.1029/2003JB002697.
Jupp, Tim, and Adam Schultz. 2000. "A Thermodynamic Explanation for Black Smoker Temperatures." *Nature* 403 (February): 880–83.
Kim, Jong-Gyun, and Milind D Deo. 2000. "Finite Element, Discrete-Fracture Model for Multiphase Flow in Porous Media." *AICHE Journal* 46 (6): 1120–30. doi:10.1002/aic.690460604.
Koide, H., and S. Bhattacharji. 1975. "Formation of Fractures around Magmatic Intrusions and Their Role in Ore Localization." *Economic Geology* 70 (4): 781–99. doi:10.2113/gsecongeo.70.4.781.
Lapwood, E. R. 1948. "Convection of a Fluid in a Porous Medium." *Proc. Camb. Phil. Soc.* 44: 508–21.
López, Dina L. 2002. "On the Interpretation of Conductive Heat Flow Anomalies Near Fault Zones." *Geothermal Resources Council Transactions* 26.
López, Dina L., and Leslie Smith. 1995. "Fluid Flow in Fault Zones: Analysis of Convective and Topographically Driven Groundwater Flow." *Water Resources Research* 31 (6): 1489–1503.
———. 1996. "Fluid Flow in Fault Zones: Influence of Hydraulic Anisotropy and Heterogeneity on the Fluid Flow and Heat Transfer Regime." *Water Resources Research* 32 (10): 3227–35.
Loucks, Robert R, and Ulrich I Petersen. 1988. "Polymetallic Epithermal Fissure Vein Mineralization , Topia , Durango , Mexico : Part II . Silver Mineral Chemistry and High Resolution Patterns of Chemical Zoning in Veins." *Economic Geology* 8 (1974): 1529–59.
Lowell, Robert P. 1975. "Circulation in Fractures, Hot Springs, and Convective Heat Transport on Mid-Ocean Ridge Crests." *Geophysical Journal International*, no. 40: 351–65.

Magri, F., S. Möller, N. Inbar, P. Möller, M. Raggad, T. Rödiger, E. Rosenthal, and C. Siebert. 2016. "2D and 3D Coexisting Modes of Thermal Convection in Fractured Hydrothermal Systems - Implications for Transboundary Flow in the Lower Yarmouk Gorge." *Marine and Petroleum Geology* 78: 750–58. doi:10.1016/j.marpetgeo.2016.10.002.

Matthai, S. K., S. Geiger, S. G. Roberts, A. Paluszny, M. Belayneh, A. Burri, A. Mezentsev, et al. 2007. "Numerical Simulation of Multi-Phase Fluid Flow in Structurally Complex Reservoirs." *Geological Society, London, Special Publications* 292 (January 2008): 405–29. doi:10.1144/SP292.22.

Matthäi, S. K., C. A. Heinrich, and T. Driesner. 2004. "Is the Mount Isa Copper Deposit the Product of Forced Brine Convection in the Footwall of a Major Reverse Fault?" *Geology* 32 (4): 357–60. doi:10.1130/G20108.2.

McClure, Mark W., and Roland N. Horne. 2014. "An Investigation of Stimulation Mechanisms in Enhanced Geothermal Systems." *International Journal of Rock Mechanics and Mining Sciences* 72. Elsevier: 242–60. doi:10.1016/j.ijrmms.2014.07.011.

Murphy, Hugh D. 1979. "Convective Instabilities in Vertical Fractures and Faults." *Journal of Geophysical Research* 84 (B11): 6121. doi:10.1029/JB084iB11p06121.

Nield, D. A. 1968. "Onset of Thermohaline Convection in a Porous Medium." *Water Resources Research* 4 (3).

Nield, D. A., and A. Bejan. 2006. *Convection in Porous Media*. 5th ed. New York.

Pedersen, Tom, and Knut Bjørlykke. 2007. "Fluid Flow in Sedimentary Basins: Model of Pore Water Flow in a Vertical Fracture." *Basin Research* 6 (1 994): 1–1.

Pollard, David D, and Atilla Aydin. 1988. "Progress in Understanding Jointing over the Past Century." *Geological Society of America Bulletin* 100: 1181–1204.

Pribnow, Daniel, and Rüdiger Schellschmidt. 2000. "Thermal Tracking of Upper Crustal Fluid Flow in the Rhine Graben." *Geophysical Research Letters* 27 (13): 1957–60.

Rabinowicz, Michel. 1999. "Thermal Convection in a Vertical Permeable Slot: Implications for Hydrothermal Circulation along Mid-Ocean Ridges." *Journal of Geophysical Research* 104: 29,275-29,292. doi:10.1029/1999JB900259.

Rummel, F. 1991. "Physical Properties of the Rock in the Granitic Section of Borehole GPK1, Soultz-Sous-Forêts." *Geothermal Science & Technology* 3 (No. 93 (1-4)): 199–216.

Siffert, Deborah, Sébastien Haffen, Michel H. Garcia, and Yves Géraud. 2013. "Phenomenological Study of Temperature Gradient Anomalies in the Buntsandstein Formation, above the Soultz Geothermal Reservoir, Using TOUGH2 Simulations." *Proceedings of the 38th Workshop on Geothermal Reservoir EngineeringThirty-Eighth Workshop on Geothermal Reservoir Engineering*, 9. http://pangea.stanford.edu/ERE/db/GeoConf/papers/SGW/2013/Siffert.pdf.

Simms, Michael A., and G. Garven. 2004. "Thermal Convection in Faulted Extensional Sedimentary Basins: Theoretical Results from Finite-Element Modeling." *Geofluids* 4: 109–30. doi:10.1111/j.1468-8115.2004.00069.x.

Sorey, M. L. 1978. "Numerical Modeling of Liquid Geothermal Systems." *Geohydrology of Geothermal Systems*.

Taron, Joshua, and Derek Elsworth. 2009. "Thermal-Hydrologic-Mechanical-Chemical Processes in the Evolution of Engineered Geothermal Reservoirs." *International Journal of Rock Mechanics and Mining Sciences* 46 (5). Elsevier: 855–64. doi:10.1016/j.ijrmms.2009.01.007.

Tomlinson, Richard Henry. 2006. "Understanding Hydrothermal Fluid Flow Within Faults and Associated Mineralization Using a Combined Field and Numerical Approach." Imperial College London.

Tournier, Cécile, Pierre Genthon, and Michel Rabinowicz. 2000. "The Onset of Natural Convection in Vertical Fault Planes: Consequences for the Thermal Regime in Crystalline Basementsand for Heat Recovery Experiments." *Geophysical Journal International* 140 (3): 500–508. doi:10.1046/j.1365-246X.2000.00041.x.

Wangen, Magnus. 1997. "Non-Rayleigh Convection Caused by Ground Surface Topography."

Transport in Porous Media 26: 299–318.
Waring, Gerald. 1983. "Thermal Springs of the United States and Other Countries of the World - a Summary." *Geological Survey Professional Paper*, 492.
Witherspoon, P. A., J. S. Y. Wang, K. Iwai, and J. E. Gale. 1980. "Validity of Cubic Law for Fluid Flow in a Deformable Rock Fracture." *Water Resources Research* 16 (6): 1016–24. doi:10.1029/WR016i006p01016.
Yang, J., R. R. Large, and S. W. Bull. 2004. "Factors Controlling Free Thermal Convection in Faults in Sedimentary Basins : Implications for the Formation of Zinc – Lead Mineral Deposits." *Geofluids*, 237–47.
Yang, Jianwen, K. Latychev, and R. N. Edwards. 1998. "Numerical Computation of Hydrothermal Fluid Circulation in Fractured Earth Structures." *Geophysical Journal International* 135 (2): 627–49. doi:10.1046/j.1365-246X.1998.00669.x.
Yapparova, Alina, Stephan Matthäi, and Thomas Driesner. 2014. "Realistic Simulation of an Aquifer Thermal Energy Storage: Effects of Injection Temperature, Well Placement and Groundwater Flow." *Energy* 76: 1011–18. doi:10.1016/j.energy.2014.09.018.
Zhang, Lianyang, and Herbert H Einstein. 2010. "The Planar Shape of Rock Joints." *Rock Mechanics and Rock Engineering*, no. 43: 55–68. doi:10.1007/s00603-009-0054-0.